2-D Modeling of the Impact of Changing Hydraulic Parameters on the Flow Pattern at Right-angled Open Channel Confluences

Reda M. Abd El-Hady Rady[1]

[1]Associate Professor, Hydraulics Research Institute, National Water Research Center, Egypt

Abstract

In fluvial networks, confluences are inevitable and produce significant flow changes. Its presence is vital for the ecological connectivity, flood control, navigation, water quality, etc. Thus, analysis of flow behavior at the confluence of two natural rivers or two artificial channels is of special importance. Flow behavior at the channel confluence area depends on various variables. In this paper, Fluent-2D numerical model was used to simulate and evaluate the effect of three different and most influential parameters; namely; discharge ratio, width ratio, and downstream Froude number on the flow pattern and the flow separation zone dimensions at right-angled open channel confluences. To accomplish this, the model was validated using the experimental data collected by (Weber et al., 2001) on a 90 degrees channel confluence. The Validation process yielded a fair comparison between simulated and experimentally determined velocity and water surface profiles. After validation, the open channel confluence was modeled with various width and discharge ratios as well as with different Froude numbers. It was observed that increasing the distributed discharge ratio decreased the length and width of the separation zone. The results also indicated that convergence of the tributary channel reduced streamwise flow velocity in the main channel and decreased separation zone dimensions. On the other hand, the model results revealed that increasing the value of Froude number decreased the dimensions of separation zone. Despite having 3D characteristics in most cases, the results of this research showed that a much simpler and computationally effective 2D numerical model is also capable of detecting most important features of flow in confluences, including separation zone and zone of high-velocity. The results suggested that Fluent-2D can be promising tool for designing the layout of lateral intakes and outlets or the study of alluvial river bifurcations.

Keywords: Channel Confluence; Fluent-2D; Discharge Ratio; Width Ratio

1. INTRODUCTION

Natural rivers generally consist of a main channel and some tributaries. The intersection of a tributary and the main stream is often called a confluence. Confluence of two streams is a common occurrence in many hydraulic engineering problems. Typical examples are natural river networks, irrigation and drainage networks, water treatment facilities and fish passage conveyance structures. Hydrodynamics of confluences is very complicated because there are numerous factors affecting flow characteristics at the confluence. One set of variables can be described as geometry variables, such as size, shape, slope, and the angle between two channels. Many combinations of these factors are probable. A second set of parameters are flow properties such as material properties, kinematic properties, dynamic properties, and thermodynamic properties.

Combining of two flows accompanies many complex problems such as local sedimentary, channel scour and sidewall erosion and others. Some of distinctive characteristics of a confluence flow in an open channel are illustrated in Fig.1. These characteristics entail a zone of separation immediately downstream of the confluence branch channel, a contracted flow region in the main channel due to the separation zone, a stagnation point immediately upstream of the confluence, a shear plane developed between the two combining flow, and an increase in depth from the downstream channel to the upstream contributing channels (Best, 1987). The zone of separation results due to the momentum of the lateral branch flow causing the main flow to detach at the downstream corner of the confluence. Due to a number of important flow phenomena involved, many studies have been conducted to seek the detailed hydrodynamic characteristics of complex confluence flow.

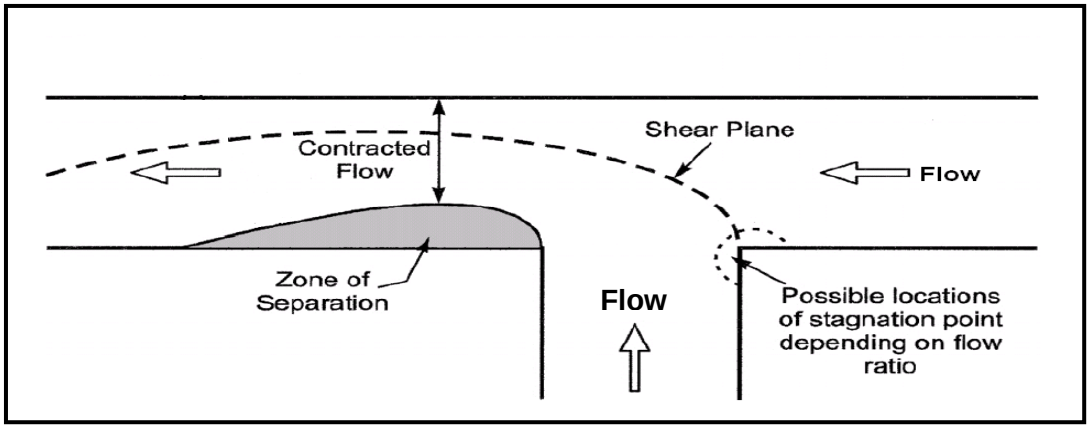

Figure 1: Flow characteristics in open channel confluence after (Best, 1987).

While open channel confluences are present in many hydraulic problems, only limited studies have been made to address this topic. Most of the researches are based on field investigations or experimental studies and a few numerical models have been developed.

Taylor (1944) was probably the first to apply an analytical model to open-channel confluence flows. His model was capable of predicting tributary channel depth upstream of the confluence. Lin and Soong (1979) investigated the energy losses encountered in a 90^o confluence. Best and Reid (1984) performed an experimental study of confluence flows with varying confluence angles and discharge ratios. They concluded that both the maximum width and length of separation zone were increased with the confluence angle and the ratio of lateral to total discharge. Best (1987) proposed a generalized model of flow at open channel confluence that consists of six different zones, namely, regions of flow stagnation, flow deflection, flow separation, maximum velocity, flow recovery, and shear layers. The zone of separation develops due to momentum of the lateral branch flow causing the main flow to detach at the downstream corner of the confluence. Mamedov (1989) developed a completely empirical approach to relate the length and width of separation zone to the confluence angle, the momentum ratio, the approach velocity ratio, and a factor depending on the approach conditions. Weerakoon et al. (1991) have presented a three dimensional model for a particular confluence structure. A standard k-ε turbulence model was used to compute the flow pattern in the confluence. Gurram et al. (1997) explored the main flow features of subcritical confluence flows. Simple confluences with confluence angles of 30^o, 60^o, and 90^o were tested. The main emphasis was put on determining the characteristics of the lateral flow and the flow contraction in the tailwater branch.

Hsu et al. (1998) described a one dimensional approach to predict the water depth upstream of the 90^o equal-width confluence for a subcritical open channel. They were able to estimate the contraction coefficient at maximum flow constriction. Shumate (1999) conducted an extensive experimental study on 90^o open channel confluence flows for the purpose of providing a complete data set that can be used for numerical code validation. Weber et al. (2001) studied a 90^o, sharp-edged, open-channel confluence for channel of equal width based on a physical model. They defined the distinctive characteristics of a sharp-edged confluence, almost the same as those of (Best, 1987). They indicated that the extensive measurements from their study provide a benchmark experimental data set that can be used for validation of numerical models.

Hsu et al. (2002) conducted a physical model for subcritical, equal-width, right-angled dividing open channel flow over a horizontal bed. Based on experimental observations, they expressed the energy-loss coefficient of a division in terms of discharge ratio, upstream Froude number, and depth ratio. Shabayek et al. (2002) developed a one-dimensional theoretical model for subcritical flows in combining open channel confluences. Their model is based on applying the momentum principle in the streamwise direction to two control volumes in the confluence together with overall mass conservation. One of the rare numerical studies on channel confluences was done by Huang et al. (2002). They developed a three-dimensional numerical model to investigate the open channel confluence flow with fixed boundaries. They validated their model with experimental data and compared it with classical one-dimensional water surface calculations.

Generally, 2D models are more enhanced than 1D numerical models and less expensive than 3D models for solving practical problems. In this research, Fluent-2D numerical model was used to investigate hydrodynamics of right-angled channel confluences over Cartesian grids. The effect of turbulence shear stresses are also incorporated in the model by an eddy-viscosity approach. A single-block strategy is used to model the whole channel, including the main and tributary channels. Experimental data of (Weber et al., 2001) was utilized for verification of the model. The effects of various prominent parameters such as discharge ratio, width ratio and downstream Froude number on hydrodynamics of confluence were then investigated. The results of this study indicated that a less complicated 2D numerical model (Fluent-2D), rather than a computationally expensive 3D one, is capable of capturing the most important velocity field zones at the confluence.

2. EXPERIMENTAL SETUP

Weber et al (2001) performed laboratory experiments in a 90° combining flow flume as shown in Fig. 2. Header tanks on both the main and branch channels supplied the varying discharge. Perforated plates and 100 mm thick honeycomb were placed at the main and branch channel inlets to cut down turbulence from pumped flows. To minimize losses on bends the channel transition piece were made smooth from vertical to horizontal and the floor of the entire facility was kept horizontal. The main channel is 21.95 m long and the confluence occurs at a distance of 5.49 m downstream the flume entrance. The branch channel is 3.66 m long. The cross section of both the branch channel and the downstream combined flow channel are all 0.91 m in width and 0.51 m in height. The total combined flow of 0.17 m^3/s and the downstream water depth of 0.30 m at the end of the main channel, were held constant, yielding a constant downstream Froude number of 0.37 and a constant downstream average velocity 0.63 m/s. Volumetric measurements were made with manometer readings from calibrated 0.203 m orifices in each of the 0.305 m supply pipes. The tailwater depth in the downstream channel was controlled by an adjustable tailgate. The coordinate system defined for this testing has the positive *x*-axis oriented in the upstream direction of the main channel. The positive *y*-direction points to the main channel wall opposite the channel confluence. The origin from which all points were measured was the bed at the upstream corner of the channel confluence. All distances were normalized by the channel width, W = 0.91 m. The dimensionless coordinates are called x*, y* for x/W, y/W, respectively.

All test sections in that study were denoted by the distance in channel widths measured positive in the x-direction for upstream main channel measurements, negative in the x-direction for combined downstream flow measurements, or negative in the y-direction for measurements in the branch channel. Velocity measurements were taken using an acoustic Doppler velocimeter with an accuracy of ±1%. The velocity measurements were also normalized by the downstream average velocity, U = 0.63 m/s. The upstream main channel, branch channel, and combined downstream water flows were denoted as Q_m, Q_b, and Q_t, respectively. The flow or discharge ratio, q*, is defined as the ratio of the upstream main channel flow to the total flow. The flow fields with six different discharge ratios of 0.08, 0.25, 0.42, 0.58, 0.75, and 0.92 were tested. The flow conditions tested are illustrated in Table1. Only q* equals to 0.42 and 0.92 were selected for model validation.

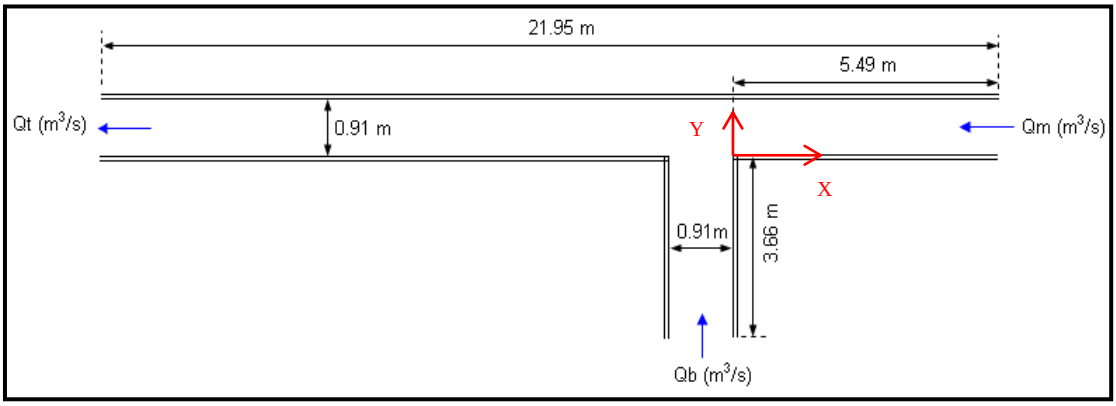

Figure2: Plan view of the test facility (Weber et al., 2001).

Table1: Experimental flow conditions (Weber et al., 2001).

Q_m (m^3/s)	Q_b (m^3/s)	Q_t (m^3/s)	$q^*=Q_m/Q_t$
0.014	0.156	0.170	0.083
0.042	0.127	0.170	0.250
0.071	0.099	0.170	0.420
0.099	0.071	0.170	0.583
0.127	0.042	0.170	0.750
0.156	0.014	0.170	0.920

3. NUMERICAL MODEL

As a result of the limitation of experimental data (Weber et al., 2001) for testing the effect of different channel width and discharge ratios on the flow pattern, the channel was numerically modeled using Fluent-2D. Fluent is the CFD solver for choice for complex flow ranging from incompressible (transonic) to highly compressible (supersonic and hypersonic) flows. Fluent governing equations sequentially use the control volume method. The governing equations are integrated over each control volume to construct discrete algebraic equations for dependent variables. These discrete equations are linearized using an implicit method. As the governing equations are nonlinear and coupled, iterations are needed to achieve a converged solution. Turbulent flows are simulated in Fluent using the standard *k-ε*, LES, RNG, or the Reynolds-stress (RSM) closure schemes. The model optimizes computational efficiency by allowing the user to choose between various spatial (Second-order upwind, third-order, QUICK) discretization scheme.

3.1. Governing Equations

The governing equations of fluid flow in rivers and channels are generally based on three-dimensional Reynoldes averaged equations for incompressible free surface unsteady turbulent flows as follows (Taylor, 1944):

$$\frac{\partial U_i}{\partial t} + U_j \frac{\partial U_i}{\partial x_j} = \frac{1}{\rho}\frac{\partial}{\partial x_j}\left[\left(-P + \frac{2}{3}k\right)\delta_{ij} + \nu_T\left(\frac{\partial U_i}{\partial x_j} + \frac{\partial U_j}{\partial x_i}\right)\right] \quad (1)$$

Where:

U_i = velocity in the x_i direction; t = time; ρ = density of flow; P = total pressure; k = turbulent kinetic energy; δ_{ij} = Kronecker delta; ν_T = turbulent viscosity; and i, j=1, 2, 3.

There are basically five terms: a transient term and a convective term on the left side of the equation. On the right side of the equation there is a pressure/kinetic term, a diffusive term and a stress term. In the current research, incompressible flow with constant properties throughout the computational domain (density and viscosity coefficient) was used. The governing differential equations of mass and momentum balance for unsteady free surface flow can be expressed as (Rodi, 1993) and (Fluent user's guide manual, 2003):

$$\frac{\partial u_i}{\partial x_i} = 0 \quad (2)$$

$$\frac{\partial u_i}{\partial t} + u_j \frac{\partial u_i}{\partial x_j} = -\frac{1}{\rho}\frac{\partial P}{\partial x_i} + g_{xi} + \nu\nabla^2 u_i \quad (3)$$

Where v is the molecular viscosity and g_{xi} is the gravitational acceleration in the x_i direction. In the current study, only the steady state condition was considered, therefore equations (2) to (3) incorporate appropriate initial and boundary conditions deployed to achieve equilibrium conditions.

3.2. The Standard K-ε Model

In the standard k-ε turbulence model, Reynolds stresses in the Reynolds-average Navier –Stokes equations are modeled by the product of an isotropic eddy viscosity and the local rate of strain. The eddy viscosity is obtained from the product of local turbulence length and velocity scales. The turbulence velocity scale is represented by $k^{1/2}$, where k is the turbulence kinetic energy per unit volume, and the turbulence length scale is determined from ε, the turbulence kinetic energy dissipation rate per unit volume. Both k and ε are derived from transport equations, which are closed by using a number of semi-empirical procedures in which standard constants are employed. The simplest and most widely used two-equation turbulence model is the k-ε model that solves two separate equations to allow the turbulent kinetic energy and dissipation rate to be independently determined.
The turbulence kinetic energy, k, is modeled as:

$$\frac{\partial k}{\partial t} + U_j \frac{\partial k}{\partial x_j} = \frac{\partial}{\partial x_j}\left(\frac{v_T}{\sigma_k}\frac{\partial k}{\partial x_j}\right) + P_k - \varepsilon \tag{4}$$

Where P_k is given by:

$$P_k = v_T \frac{\partial U_j}{\partial x_i}\left(\frac{\partial U_j}{\partial x_i} + \frac{\partial U_i}{\partial x_j}\right) \tag{5}$$

$$v_T = c_\mu \frac{k}{\varepsilon^2} \tag{6}$$

The dissipation of k is denoted ε, and modeled as:

$$\frac{\partial \varepsilon}{\partial t} + U_j \frac{\partial \varepsilon}{\partial x_j} = \frac{\partial}{\partial x_j}\left(\frac{v_T}{\sigma_\varepsilon}\frac{\partial \varepsilon}{\partial x_j}\right) + C_{\varepsilon 1}\frac{\varepsilon}{k}p_k + C_{\varepsilon 2}\frac{\varepsilon^2}{k} \tag{7}$$

The constants in the k-ε model have the following values: $c_\mu = 0.09$, $C_{\varepsilon 1} = 1.44$, $C_{\varepsilon 2} = 1.92$, $\sigma_k = 1.0$, and $\sigma_\varepsilon = 1.30$

3.3. Boundary and Initial Conditions

A 10 × 5 cm mesh was used for the computational grid. To focus on post confluence flow and investigate its effect on upstream and downstream flow, a finer mesh was used. To achieve this, the area around the confluence of the two streams had 2.5 cm grid size in the longitudinal direction. Fig. 3 shows a two-dimensional view of the final mesh. Since rectangular elements were used, the element size, especially in the interface, was changed gradually. The elements were also checked for overlapping.

For both channels mean velocity was specified as channel inlet boundary conditions depending on the width and discharge ratios. Static pressure was imposed as an outlet boundary condition. Downstream depth had a constant value in all models, which was similar to the experimental model except for the case of increasing Froude number. No-slip conditions and smooth roughness were imposed on the walls (channel floor and sides), which were similar to the experimental channel. Finally, to govern the free surface condition, an opening boundary condition was imposed on the model. The Volume of Fluid (VOF) method was used to calculate the water level in the process of iteration (Liu and Yang, 2013).

After specifying the type of mesh and boundary conditions, the numerical model was initiated to solve the two phases of flow variables (water + air) by extrapolating from the interior solution domain. The solution process stopped automatically when all normalized governing equations reached 10^{-7}. In addition to studying the effect of discharge ratio, which was the main parameter in previous experimental study, the effect of two other parameters including width ratio and downstream Froude number were also studied. For the validation process two discharge ratios of 0.42 and 0.92 were used.

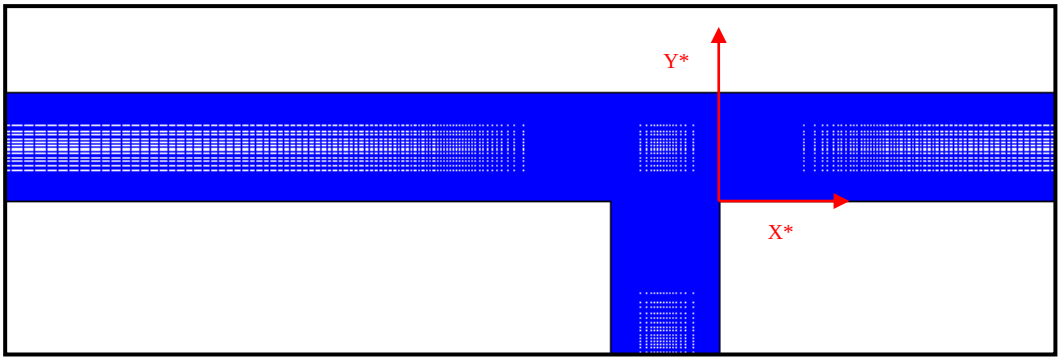

Figure 3: Computational geometry and grid.

4. MODEL VALIDATION

To verify the numerical results and evaluate the reliability of using them where experimental data were not available, it was necessary to validate the proposed numerical model. To do this, the simulated and experimental results were compared and the simulated error was estimated. The experimental results of Weber et al. (2001) served to validate the numerical simulation. Figs. 4 to 11 illustrate a comparison between the measured and simulated u* values, where u* is the dimensionless velocity, i.e. u/downstream average velocity. In these figures, the velocity profiles of flow were compared for two discharge ratios of q* = 0.42 and 0.92. The comparisons were made for X* = −1, −1.5, −2 and −3 and longitudinal cross sections of Y* = 0.25 and 0.67. In Figs. 12 to 15 results of the numerical model with respect to water surface profile were compared to those of (Weber et al., 2001) for the same discharge ratios. According to Figs. 4 to 11, the simulation accuracy increased with the increase in discharge ratio because of the reduction in tributary channel flow effect and reduction in the separation zone as well as recirculation flow. The average error for q* = 0.42 was found to be 9 %, whereas, for q* = 0.92, an average error of 4% was obtained. Thus, compared to q* = 0.42, the simulation was more accurate for q* = 0.92. The separation zone developed in the vicinity of the inner wall of the main channel downstream of the confluence, reducing the effective width of the channel, which increased the flow velocity. Therefore, by increasing the size of the separation zone, the maximum velocity increased as well.

For both discharge ratios, the error was maximum at about X* = −1.5 where the separation zone had the largest width. The maximum simulation error was 21%. It decreased by moving up along the channel and reduced to about 10% for X* = −3. The Root Mean Square Error was obtained to be 0.052 for longitudinal velocity. The correlation coefficient and regression slope were estimated as 0.94 and 0.97, respectively, which shows that the model is accurately calibrated and the model's capability to simulate the velocity is very good. In general, considering the fact that the approximate error was about 6%, the numerical model was found to be suitable. The model also proved to have good ability to predict water surface profile (Figs. 12 to 15).

The maximum difference between experimental data and simulation results was at the right bank of main channel, which is the position of separation zone. From all above, it can be concluded that model results are generally in agreement with measured ones, except for some sections, which might be partly due to the three-dimensional effects. Moreover, due to limitation of 2-d numerical model the vertical acceleration was neglected in the current 2D- study.

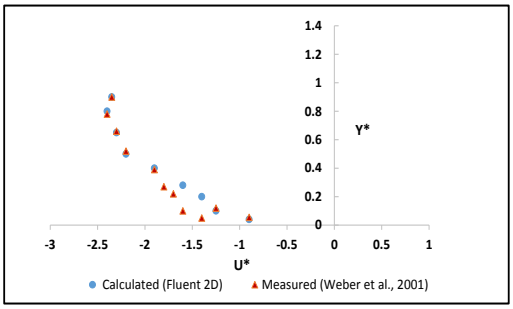

Figure 4: X-Velocity profile of main channel (X* = -1 and q* = 0.92).

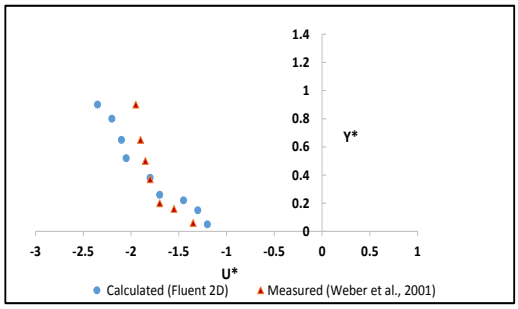

Figure 5: X-Velocity profile of main channel (X* = -1 and q* = 0.42).

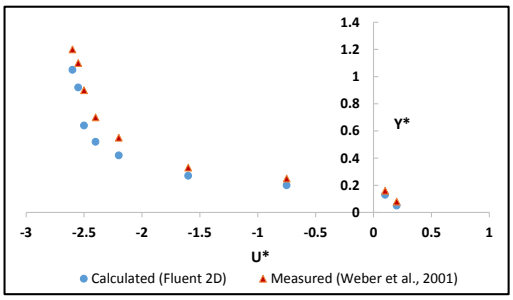

Figure 6: X-Velocity profile of main channel (X* = -1.50 and q* = 0.92).

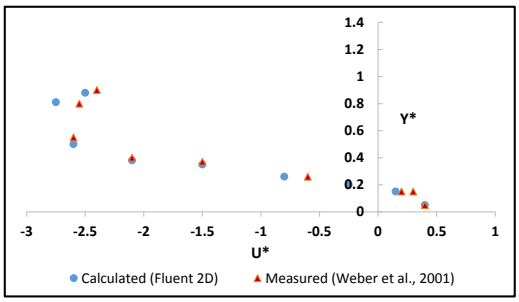

Figure 7: X-Velocity profile of main channel (X* = -1.50 and q* = 0.42).

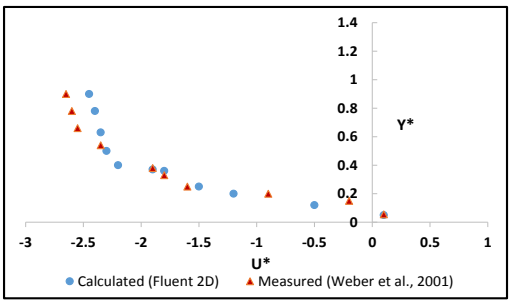

Figure 8: X-Velocity profile of main channel (X* = -2.00 and q* = 0.92).

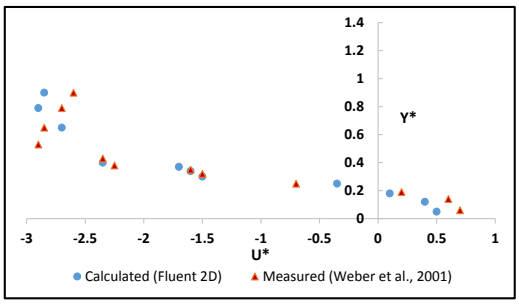

Figure 9: X-Velocity profile of main channel (X* = -2.00 and q* = 0.42).

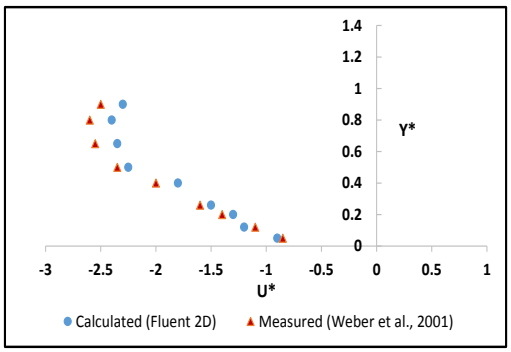

Figure 10: X-Velocity profile of main channel (X* = -3.00 and q* = 0.92).

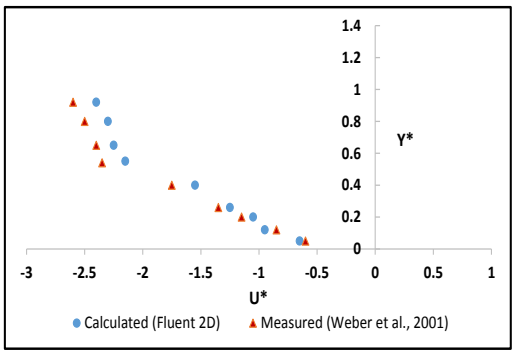

Figure 11: X-Velocity profile of main channel (X* = -3.00 and q* = 0.42).

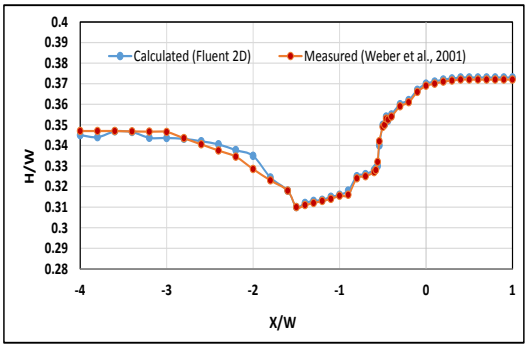

Figure 12: Water surface profile (Y* = 0.25 and q* = 0.92).

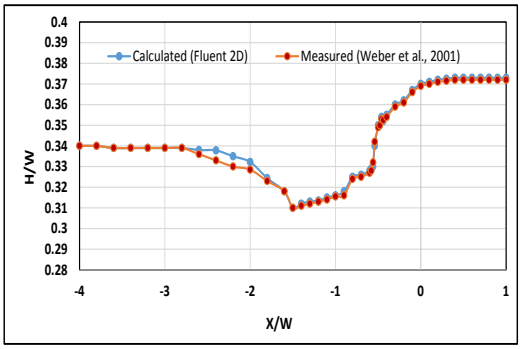

Figure 13: Water surface profile (Y* = 0.67 and q* = 0.92).

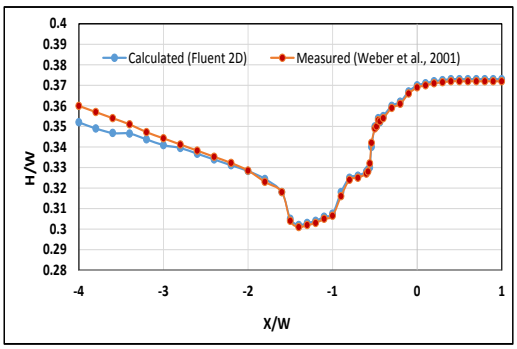

Figure 14: Water surface profile (Y* = 0.25 and q* = 0.42).

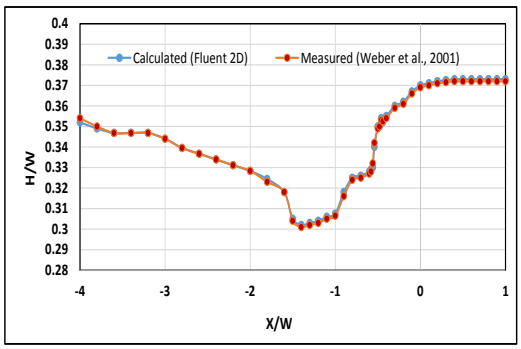

Figure 15: Water surface profile (Y* = 0.67 and q* = 0.42).

5. RESULTS AND DISCUSSION

After validating the model for 90^o confluence using experimental data, the model was then applied to investigate the effects of discharge ratio, width ratio, and downstream Froude number on the flow field. The channel flow was simulated and analyzed for width ratios (W*) of 1.0, 1.25, 1.5, and 2.50, where W* is defined as the ratio of the branch channel width to the main channel width, Froude numbers of 0.37, 0.50, 0.65, and 0.75, and discharge ratios of 0.083, 0.25, 0.42, 0.58, 0.75, and 0.92.

5.1. Effect of Discharge Ratio

The effect of varying discharge ratios same as used in experimental tests (0.083, 0.25, 0.58, and 0.75) with average simulation errors of 9.8, 9.5, 6.2, and 5.5 %, respectively on flow pattern is demonstrated in Fig. 16. Part of the model results of velocity distribution for discharge ratios of 0.42 and 0.92 was already illustrated in Figs. 4 to 11. The longitudinal velocity u* is the dimensionless velocity in the x-axis direction, i.e. u/downstream average velocity. Note that according to coordinate axes defined earlier, negative values for velocities indicate flow in mainstream direction. The separation zone can be seen as the area of positive velocities along the lower bank, immediately downstream of the confluence. Recirculation inside the separation zone is shown as the region of positive velocity approximately between x* = -1 and x* = -3 in the main channel, indicating upstream motion. A region of high velocities occurs just downstream of the confluence approximately between x* = -1.5 and x* = -3 in the main channel, since the separation zone contracts the flow. Fig. 16 elucidates the structure of the combining streams and the zone of flow separation downstream the main channel.

The momentum of the lateral branch flow caused the main flow to detach at the downstream corner of the confluence. This is more significant for lower (q*) flow condition. As a result, the water depth rose up at the upstream of the main channel. For low discharge ratio flows, more momentum comes from tributary channel resulting in complex flow downstream of the confluence (Fig. 16). Moreover, the model results show that higher (q*) will take shorter distance downstream from the confluence to reach

uniform flow condition again. For more analysis, the water surface profile for two different y*=y/W values was processed for these discharge ratios. Figs. 12 to 15 show that there is a drop in water surface profile just after the confluence. It is clear, the difference between upstream and downstream water levels is less for q*=0.92 compared to corresponding value for q*=0.42.

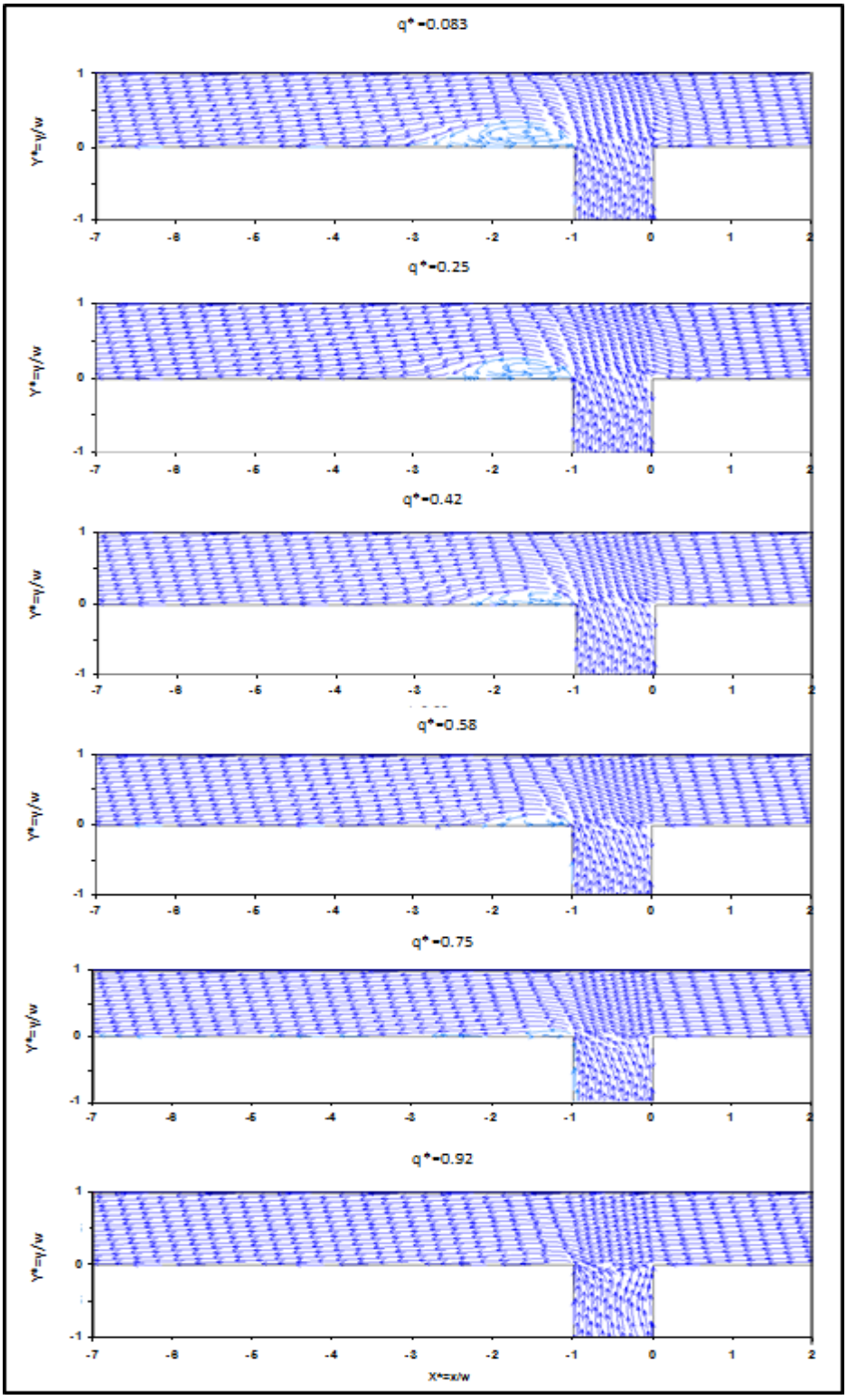

Figure 16: 2D Streamlines plot for different q*.

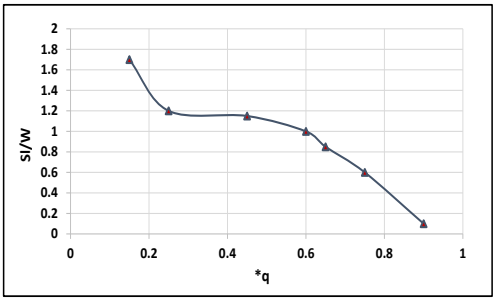

Figure 17: Relation between discharge ratio and dimensionless separation zone length.

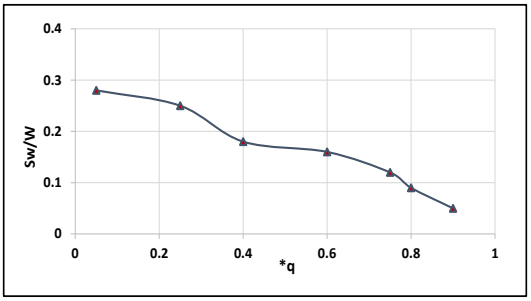

Figure 18: Relation between discharge ratio and dimensionless separation zone width.

Figs. 17 and 18 present the predicted variation of dimensionless maximum length (S_L) and width (S_w) of separation zone in the main channel for different discharge ratios, respectively. Results indicated that both length and width of the separation zone decrease with increasing discharge ratio. Increasing discharge ratio results in decreasing the tributary discharge, and hence the main stream discharge dominates the flow field. It can be seen that for a lower discharge ratio, more than 25% of the downstream main channel width is occupied by the recirculation zone.

5.2. Effect of Width Ratio

In this research, the effect of convergence of branch channel on flow pattern and separation zone was studied. The discharge ratio was kept at 0.92 for this case in order to maintain the highest possible momentum in branch channel. Figs. 19 to 22 show the impact of widening the branch channel on velocity profiles. The velocity distribution due to convergence of the branch channel reduces stream wise flow velocity in the main channel because by increasing the inlet width of branch channel, the momentum and velocity of lateral channel decreases and the main channel flow is not strongly influenced by lateral flow. In the same context, the effect of convergence of branch channel on water surface profile was examined and results are demonstrated in Fig. 23. The figure shows that by increasing the width ratio the difference between upstream and downstream flow depths at confluence area decreases. On the other hand, Figs. 24 and 25 illustrate the impact of branch channel convergence on separation zone dimensions. It can be noticed that both separation length and width decrease with increasing the width ratio. Increasing the width ratio led to a decrease in the velocity magnitude in the tributary channel. A decrease in tributary velocity led to a decrease in the main channel's separation zone. The contraction zone velocity reduced as the separation zone became smaller.

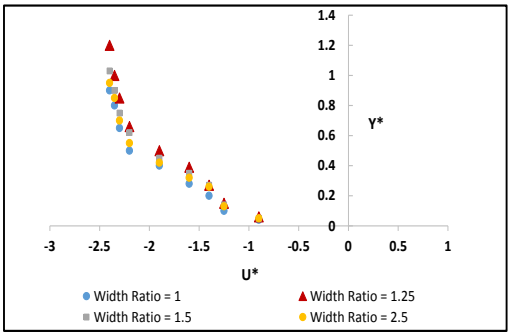

Figure 19: Velocity profile of main channel for different width ratios (X*= -1).

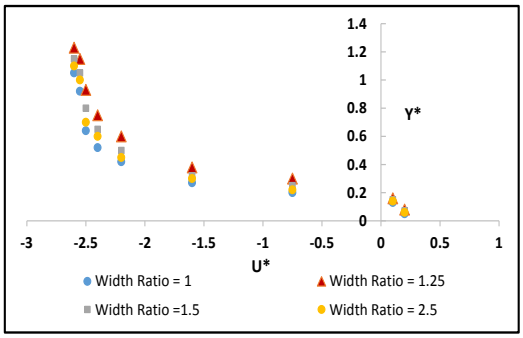

Figure 20: Velocity profile of main channel for different width ratios (X* = -1.5).

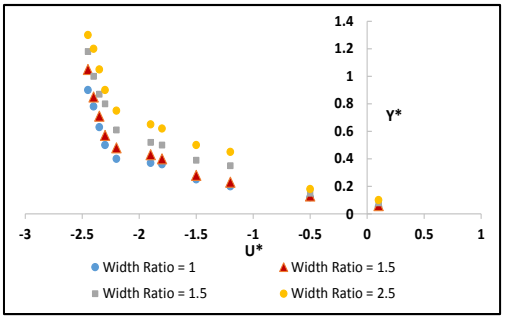

Figure 21: Velocity profile of main channel for different width ratios (X* = -2).

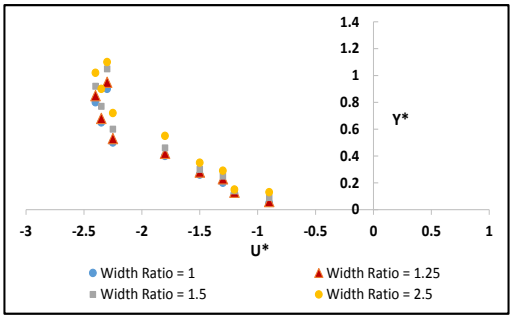

Figure 22: Velocity profile of main channel for different width ratios (X* = -3).

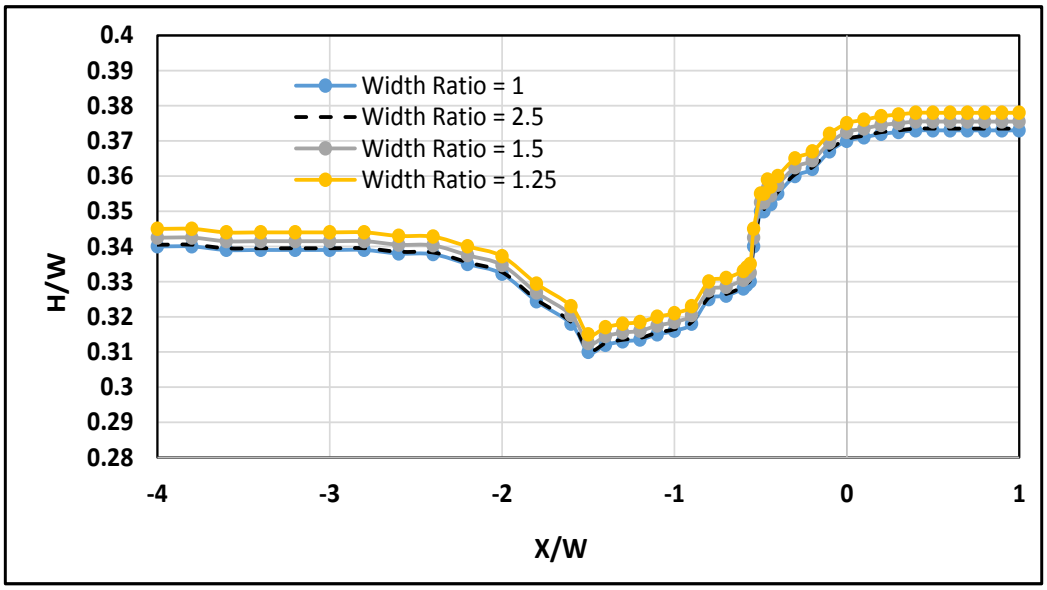

Figure 23: Water surface profile for different width ratios (Y* = 0.67).

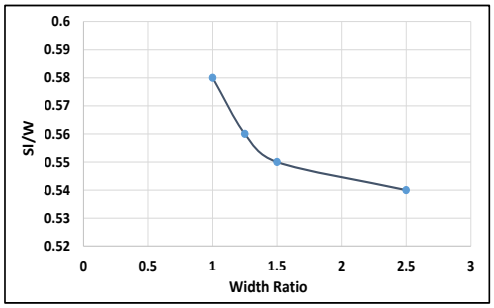

Figure 24: Relation between width ratio and dimensionless separation zone length.

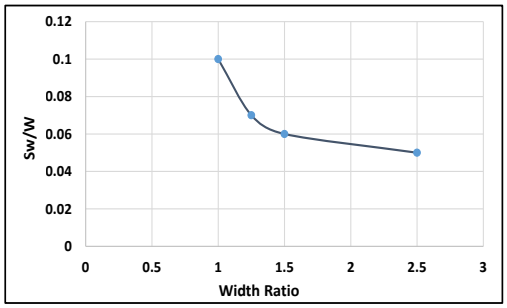

Figure 25: Relation between width ratio and dimensionless separation zone width.

5.3. Effect of Froude Number

As mentioned earlier, downstream Froude number was kept at Fr =0.37 in the simulations reported in Sections 5.1 and 5.2. In this section, three other downstream Froude numbers, i.e. Fr = 0.5, Fr = 0.65, and Fr = 0.75 were also investigated to study the effect of this parameter on the flow field. The discharge ratio was kept as q*=0.92 and the width ratio as one. The simulation results showed that dimensions of separation zone, particularly its width, decreased with increasing the value of Froude number .Fig. 26 presents the simulated water surface profiles for different values of Froude number. As the figure shows, the water level drop is decreased by increasing downstream Froude number.

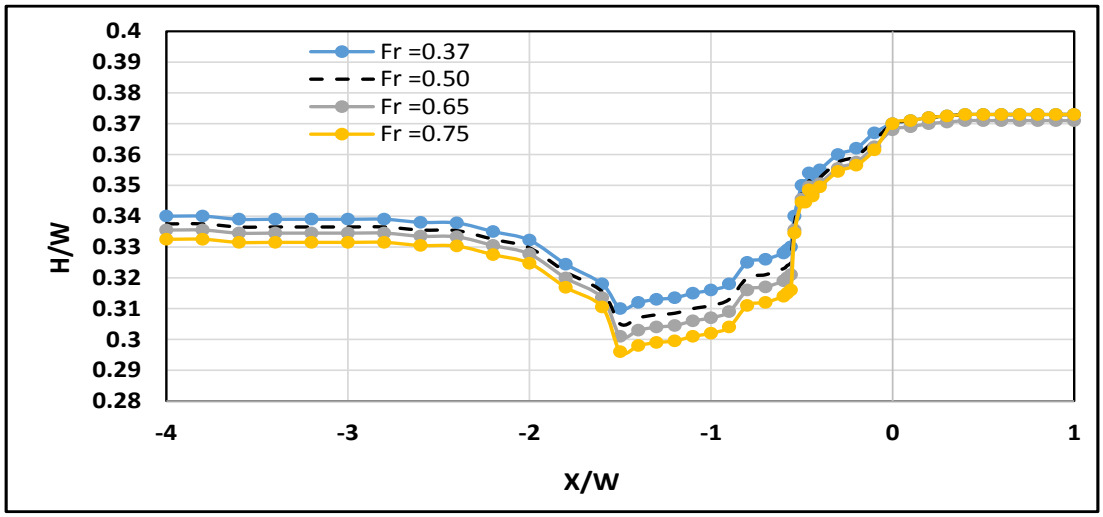

Figure 26: Water surface profile for different Froude numbers (Y* = 0.67)

6. CONCLUSIONS AND RECOMMENDATIONS

In this paper, the effects of discharge ratio, width ratio, and downstream Froude number on characteristics of flow at a 90 degrees confluence were investigated. Fluent-2D was used to model these effects. The numerical model was first verified using the experimental study results of Weber et al. (2001) and then different scenarios of discharge ratio, width ratio, and Froude number were tested. The results showed that the 2D numerical model is capable of predicting most features of flow in confluences, such as the presence of separation zone, high-velocity zone and water level drop at the confluence. The velocity profile results for various discharge and width ratios indicated that with increasing both ratios, the size of the separation zone decreased. The entry of tributary streams to the main channel caused the main flow to deviate towards the bed, thus decreasing the depth of mixed flow just at the beginning of the main channel's downstream region. This reduction in depth was intensified by increasing the width ratio. The model results also revealed that due to a decreasing tributary flow effect on the main channel flow, increasing Froude number led to a reduced effect of the separation and contraction zones. Despite being more accurate, three-dimensional models are computationally expensive in solving real world problems. In these cases, 2D models can give enough information for practical purposes. On the other hand, while in most cases the characteristics of flow at the channel confluences are three-dimensional, studying 2D models in predicting real life problems in fluid mechanics is important. Consequently, such models can be further extended by incorporating some 3D features of flow into 2D depth-averaged equations to achieve more realistic results. It is strongly recommended to use the 2D capabilities of Fluent numerical model in investigating various designs of inlet and outfall structures of power plants as the model has the ability to well simulate the turbulent jet flow.

REFERENCES

1. Best, J. L., 1987. Flow dynamics at river channel confluences: Implications for sediment transport and bed morphology. *Recent Development in Fluvial Sedimentology*, Vol. 39, pp. 27-35.
2. Best, J. L. & Reid, I., 1984. Separation zone at open-channel confluences. *Journal of Hydraulic Engineering*, Vol. 110, 11, pp. 1588-1594.
3. FLUENT user's guide manual-version 6.1., Fluent Incorporated, N.H., 2003.
4. Gurram, S. K., Karki, K. S. & Hager, W. H., 1997. Subcritical confluence flow. *Journal of Hydraulic Engineering*, Vol. 123, No. 5, pp. 447-455.
5. Hsu, C. C., Wu, F. S. & Lee, W. J., 1998. Flow at 90º equal-width open channel confluence. *Journal of Hydraulic Engineering*, Vol. 124, No. 2, pp. 186-191.

6. Hsu, C. C., Tang, C.J., Lee, W. J. & Shieh, M. Y., 2002. Subcritical 90° equal-width open-channel dividing flow. *Journal of Hydraulic Engineering*, Vol. 128, No. 7, pp. 716-720.
7. Huang, J., Weber, L. J. & Lai, Y. G., 2002. Three-dimensional numerical study of flows in open-channel confluences. *Journal of Hydraulic Engineering*, Vol. 128, No. 3, pp. 268-280.
8. Lin, J. D. & Soong, H. K., 1979. Confluence losses in open channel flows. *Water Resources Research*, Vol. 15 No. 2, pp. 414-418.
9. Liu, T., & Yang, J., 2013. Three-dimensional computations of water–air flow in a bottom spillway during gate opening. *Journal of Hydraulic Research*, *8*(1), 104–115.
10. Mamedov, A. S., 1989. Hydraulic calculation of a confluence. *Hydrotechnical Construction*, Vol. 23, No. 9, pp. 553-556.
11. Rodi, W., 1993. Turbulence models and their application in hydraulics. IAHR, Delft, The Netherlands.
12. Shabayek, S., Steffler, P. & Hicks, F., 2002. Dynamic model for subcritical combining flows in channel confluences. *Journal of Hydraulic Engineering*, Vol. 128, No. 9, pp. 821-828.
13. Shumate, E. D., 1998. Experimental description of flow at an open channel confluence. Master thesis, University of Iowa, Iowa.
14. Weber, L. J., Schumate, E. D. & Mawer, N., 2001. Experiments on flow at a 90° open-channel confluence. *Journal of Hydraulic Engineering*, Vol. 127, No. 5, pp. 340-350.
15. Taylor, E. H., 1944. Flow characteristics at rectangular open-channel confluences. *Transaction ASCE*, Vol. 109, pp. 893-902.
16. Weerakoon, S. B., Kawahara, Y. & Tamai, N., 1991. Three-dimensional flow structure in channel confluences of rectangular section. *Proc., 24th IAHR Congr*ess, pp. 373-380.

LIST OF SYMBOLS

Fr	Froude number (dimensionless)
g_i, g_{xi}	gravitational acceleration in I, x_i directions (m/s^2)
H	mean flow depth (m)
K	turbulent kinetic energy ($kg/m^2\ s^2$)
P	total pressure (N/m^2)
Q_m	discharge of main channel (m^3/s)
Q_b	discharge of branch channel (m^3/s)
Q*	discharge ratio (dimensionless)
U_{xi}	velocity in the x_i direction (m/s)
U*	dimensionless velocity in main channel
S_L	maximum length of separation zone (m)
S_W	maximum width of separation zone (m)
X	distance in main channel downstream from branch channel centerline (m)
Y	distance in branch channel from opposite main channel wall (m)
W	width of both channels (m)
W*	width ratio (dimensionless)
ρ	density of fluid (kg/m^3)
ν_T	turbulent viscosity (m^2/s)